



Article

Liquid-Phase Hydrodeoxygenation of Guaiacol over Mo₂C Supported on Commercial CNF. Effects of Operating Conditions on Conversion and Product Selectivity

Rui Moreira ¹, Elba Ochoa ², José Luis Pinilla ^{2,*} , António Portugal ¹  and Isabel Suelves ²

¹ Computational, Statistics and Materials (CEM), Chemical Process Engineering and Forest Products Research Centre (CIEPQPF), Department of Chemical Engineering, University of Coimbra, 3030-790 Coimbra, Portugal; ruimoreira@eq.uc.pt (R.M.); atp@eq.uc.pt (A.P.)

² Instituto de Carboquímica, CSIC, C/Miguel Luesma Castán 4, 50018 Zaragoza, Spain; eochoa@icb.csic.es (E.O.); isuelves@icb.csic.es (I.S.)

* Correspondence: jlpinilla@icb.csic.es; Tel.: +34-976-733-977

Received: 26 February 2018; Accepted: 20 March 2018; Published: 22 March 2018



Abstract: In this work, a Mo₂C catalyst that was supported on commercial carbon nanofibers (CNF) was synthesized and tested in the hydrodeoxygenation (HDO) of guaiacol. The effects of operating conditions (temperature and pressure) and reaction time (2 and 4 h) on the conversion of guaiacol and products selectivity were studied. The major reaction products were cresol and phenol, followed by xylenols and toluene. The use of more severe operating conditions during the HDO of guaiacol caused a diversification in the reaction pathways, and consequently in the selectivity to products. The formation of phenol may have occurred by demethylation of guaiacol, followed by dehydroxylation of catechol, together with other reaction pathways, including direct guaiacol demethoxylation, and demethylation of cresols. X-ray diffraction (XRD) analysis of spent catalysts did not reveal any significant changes as compared to the fresh catalyst.

Keywords: hydrodeoxygenation; molybdenum carbide catalyst; carbon nanofibers supported catalysts

1. Introduction

Lignocellulosic bio-oils cannot be fractionally distilled for the separation of petrochemical cuts in the current oil industry infrastructure, because they repolymerize upon heating due to the chemical and thermal instability related with their high oxygen content [1,2]. Consequently, bio-oils must be further processed (upgraded) before they can be used as liquid fuel or as a source of industrial chemicals.

Liquid-phase hydrodeoxygenation (HDO) is a catalytic upgrading process that is undertaken in a wide range of pressures (2–30 MPa) and temperatures (423–723 K), where hydrogen is used to exclude excess oxygen from lignocellulosic bio-oil, with the purpose of getting a product that is chemically similar to crude [2,3]. High pressures are used to ensure adequate solubility of hydrogen in the reaction media, this way increasing its availability in the vicinity of the catalyst particles and consequently accelerating the reaction rate [2]. Conventional hydrotreating and hydrogenation (HYD) catalysts have been tested, as well as novel ones that are based on alkaline, alkaline-earth, transition, and noble metals supported in carbon or metal oxides. However, all of the catalysts suffer from irreversible deactivation that is caused mainly by coking, active phase loss, and water poisoning [2–5].

Metal carbides, nitrides, and phosphides were also attempted. Of those, carbides have recently received increased attention, as their properties resemble those of noble metal catalysts. The introduction of carbon on the lattice of transition metals leads to an increase in the lattice parameter

a, which leads to a contraction of the *d*-band [6–9]. Through carburization the *d*-electron density of transition metals increases at the Fermi level, conferring to the parent metal an electron density similar to those of noble metals, and the higher the carbon content, the higher the noble metal-like behavior of the obtained materials [6–9].

Molybdenum carbide (Mo_2C) is an excellent catalyst for the hydrogenation and hydrogenolysis of hydrocarbons [8,10]. There are three catalytically relevant molybdenum carbide phases, namely, cubic ($\delta\text{-Mo}_2\text{C}$), hexagonal ($\alpha\text{-Mo}_2\text{C}$), and orthorhombic ($\beta\text{-Mo}_2\text{C}$), following the notation convention defined by the Joint Committee on Power Diffraction Standards. A density functional theory (DFT) study revealed that the $\beta\text{-Mo}_2\text{C}$ phase has the strongest metallic and ionic character, and is highly stable due to its small work function. Its (111) and (001) surfaces are polar, while the (011), (101), and (100) surfaces are nonpolar [11]. It is particularly suitable as electrocatalyst in reducing processes, as well as heterogeneous catalyst in reactions where electron transfer is needed from the catalyst to adsorbed reactant, characteristic of bond breaking reactions [11]. Another DFT study [12] revealed that dispersive forces predict an essentially spontaneous dissociation of hydrogen molecules on $\beta\text{-Mo}_2\text{C}$ (001), independently of the surface termination. These studies show that molybdenum carbides present an interesting potential as catalyst material for HDO [8].

Metal based catalysts have been usually supported on metal oxides and zeolites, which are sometimes pointed out as the cause for catalysts deactivation [2,3,6]. Within the universe of carbon supports, carbon nanofibers (CNFs), and carbon nanotubes (CNTs) have been less exploited as catalyst supports in HDO of bio-oils [13]. CNFs and CNTs present high mechanical resistance, high electrical conductivity, high thermal stability, high conductivity, high capacity for hydrogen adsorption even at high temperatures, and a morphology that allows for the rapid access of reactants and evacuation of products from catalytic active sites [14–17]. Moreover, acid and alkali treatments can be used to enhance the hydrophilicity by creating oxygen functionalities over the carbonaceous materials, and facilitating the dispersion of metals over the CNFs with water solutions [14,15,18]. These properties of CNFs and CNTs gained the interest of the catalysis community working on HDO [13,19,20]. Supported molybdenum carbides can be synthesized by carbothermal reduction [21,22]. By this process, the Mo_2C phase is formed by using carbonaceous supports as carbon source under a hydrogen atmosphere.

Several model compounds of bio-oil that are produced by fast pyrolysis from lignocellulosic biomass have been used in literature on HDO [2–4,10]. Among them, guaiacol (2-methoxyphenol) is a suitable model compound for the evaluation of HDO catalysts, since it incorporates two different oxygen groups that are commonly present in lignin derived compounds, namely, hydroxyl ($-\text{OH}$) and methoxyl ($-\text{OCH}_3$), which hamper the complete deoxygenation of lignocellulosic bio-oils [2,4,23].

In this work, catalysts based on Mo_2C supported on commercial CNF pre-treated with nitric acid (HNO_3) were synthesized and tested in the HDO of guaiacol. The effects of operating conditions and the reaction time on the conversion of guaiacol and products selectivity were studied.

2. Results and Discussion

2.1. Support Characterization

The results of the characterization of the as received (CNF_0) and pretreated (CNF) nanofibers by N_2 -physisorption and TPD are presented in Table 1.

When comparing the CNF_0 with the CNF, it can be seen from Table 1 that the HNO_3 pretreatment did not have any impact on the pore volume or surface area of the as received material, since the differences observed lies within the equipment experimental error. In the literature [24–26], the evolution of CO_2 during TPD (Temperature Programmed Desorption) has been assigned to the existence of acid groups over carbonaceous supports caused by the decomposition of carboxylic acids, carboxylic anhydrides, and lactones upon heating, while the evolution of CO has been assigned to the presence of basic and neutral groups over such support materials that is caused by the decomposition

of phenols, ethers, quinones, and carbonyls. These oxygen groups can be created over carbonaceous supports by functionalization with acid or alkali pretreatments [24–26]. The HNO₃ pretreatment substantially increased the number of oxygen groups over the as received CNF, as shown by the evolution of CO and CO₂ during the TPD experiments and by the (almost three-fold) increase in the support oxygen content, in agreement with previous works [27,28]. The increase in the number of acid sites was two times higher than the increase in basic and neutral sites, in agreement with the results of other researchers [24]. The evolution on CO and CO₂ during the TPD experiments indicates that the majority of the oxygen groups existent over the CNF₀ were mainly neutral and basic, whereas over the CNF an almost even distribution between acid and basic/neutral groups was observed.

Table 1. Results of N₂-physisorption and Temperature Programmed Desorption (TPD) of the bare commercial nanofibers (CNFs) supports (CNF₀ = as received carbon nanofibers; CNF—pretreated carbon nanofibers).

Sample	Surface Area (m ² /g)	Pore Volume (cm ³ /g)	Pore Size (nm)	CO (mmol/g)	CO ₂ (mmol/g)	Oxygen Content (wt %)
CNF ₀	39.6	0.156	15.5	0.256	0.079	0.7
CNF	37.8	0.110	13.7	0.410	0.398	1.9
Mo ₂ C/CNF	44.2	0.147	13.3	n.d.	n.d.	n.d.

n.d.: not determined.

2.2. Fresh Catalysts Characterization

As shown in Figure 1, the XRD patterns of as received and functionalized CNF showed a prominent reflexion at ca. 26° and weak peaks at ca. 43–45° assigned to graphitic carbon. No significant changes in reflexions assigned to C were observed after the functionalization treatment that was used. Mo₂C/CNF catalyst also showed a major reflexion intensity at 26° and a minor peak at 45°, with both being assigned to the graphitic carbon phase. The same diffractograms also revealed seven small peaks assigned to the molybdenum carbide phase (Mo₂C), with reflexions detected at 2θ angles of 34°, 38°, 40°, 52°, 61°, 69°, 75°, and 76°, assigned to orthorhombic Mo₂C (lattice parameters a = 0.4724 nm, b = 0.6002 nm, c = 0.5215 nm) [11,29–33]. The size of the crystallites (interpreted here as coherent diffraction domains) estimated by XRD is ca. 11.2 nm. The molybdenum carbide crystallites in the Mo₂C/CNF catalyst are of the same order of magnitude of those that are presented in other studies on similar catalysts, having in consideration that values as lower than 3 nm [34] and as high 11.3–12.6 nm [19] have been reported. Moreover, other authors [29] synthesized Mo₂C catalysts that are supported on activated carbon (AC) using similar preparation methodology and obtained particle sizes of comparable magnitude (9–12 nm) to those that were observed in this work. No other molybdenum phases were detected by XRD in the synthesized catalysts, indicating that the solid phase carburization of the molybdenum oxide used as metal precursor was fully accomplished.

Figure 2 shows the TEM micrographs of the CNF (a and b) and Mo₂C/CNF (c and d). CNF present an average diameter of 100 nm with hollow core that was accounting almost the entire width. Mo₂C/CNF catalyst evidenced the presence of Mo₂C particles with a relatively narrow distribution between 5 and 12 nm, in agreement with XRD measurements. It can be seen that most of the catalytic particles were positioned at inner face of the CNF support. Apparently, some particles that were initially deposited at the external walls penetrated the CNF by etching channels from the surface inwards. This phenomenon has been earlier reported by other authors working on several metal-graphene composites [35–42]. It was previously reported in the literature that iron oxide particles could gasify graphene supports, opening irregular channels throughout the graphene layers during a heat treatment at 773 K under a reductive hydrogen atmosphere for 2 h [36–38]. When considering this literature information, the etching of the CNF support in the present study could have been caused by a similar phenomenon. The molybdenum oxides formed upon the thermal decomposition of the molybdate ions that were deposited on the surface of the CNF during the incipient wetness impregnation may

have gasified the graphene layers during the carburization procedure, since this heat treatment was undertaken at a higher temperature (1023 K) and equal period of time (2 h).

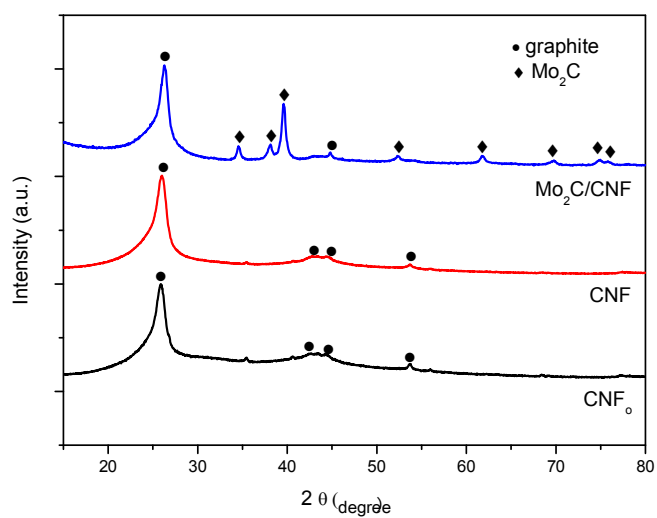


Figure 1. X-ray diffraction patterns of the catalysts.

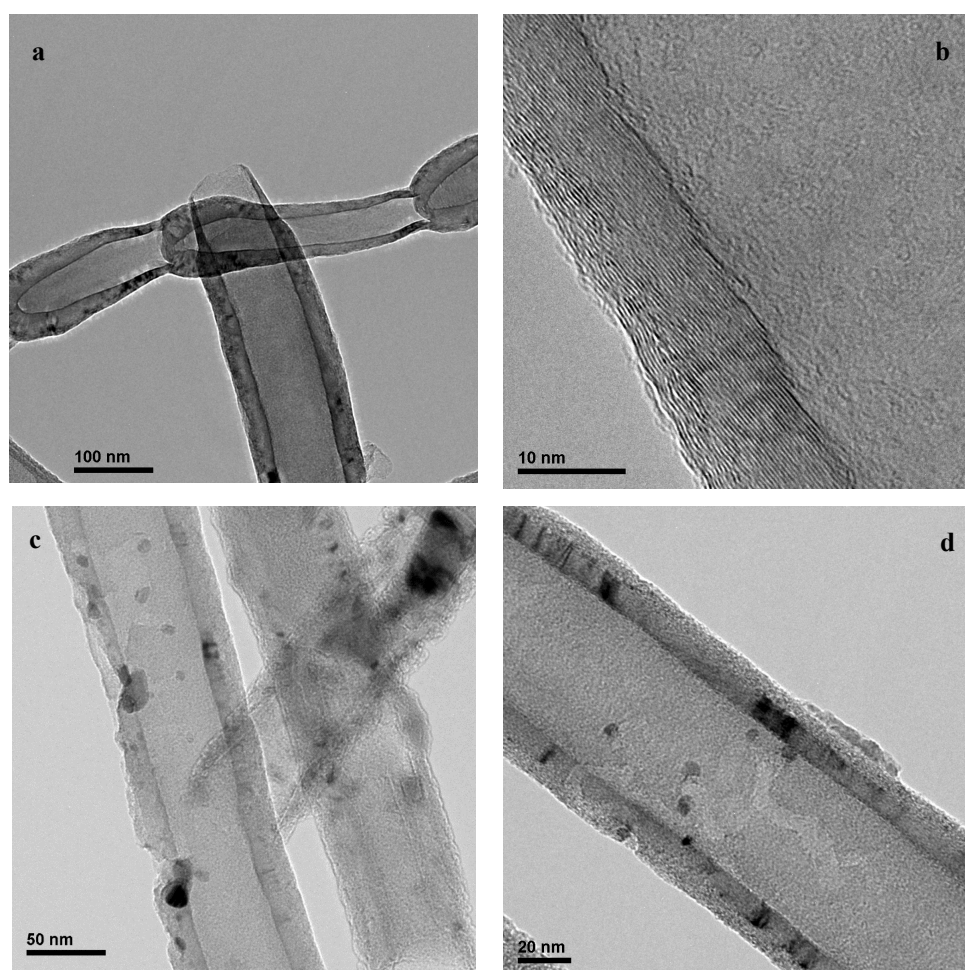


Figure 2. Transmission Electron Microscopy (TEM) micrographs of the CNF_0 (a,b) and $\beta\text{-Mo}_2\text{C}/\text{CNF}$ catalyst (c,d).

An alternative pathway for the etching of the CNF would be the catalytic hydrogenation of the graphene layers during the carbothermal reduction [38–40]. By this route, graphene was etched by deposited metal particles at annealing temperatures above 873 K in a hydrogen atmosphere. This etching mechanism would involve the dissociation of molecular hydrogen on the metal surface, followed by the reaction of the so formed elemental hydrogen with the graphene carbon into methane [38–40].

In spite of the real mechanism involved, which is out of the scope of the contribution, to the best of our knowledge, the etching of carbonaceous materials involving molybdenum is reported in the present work for the first time. It should be noted that most published works use nitrogen gas during the carburization of molybdenum carbides supported on CNF, while in this contribution, hydrogen was used instead, and this may be an important cause for the observed etching.

Another fact that might have contributed for the appearance of the catalytic particles on the inner surface of the support could be related with the high average internal diameter of the CNF that was used in this work. Other authors [43] working on Fischer Tropsch synthesis prepared cobalt catalysts supported on CNTs and CNFs with internal diameters of 60 and 20 nm, respectively, by incipient wetness impregnation, in which more than 80% of the particles were located at the inner surface of the support materials. In another research [44], the authors impregnated CNT with internal diameters of up to 20 nm using aqueous solutions of $\text{Fe}(\text{NO}_3)_3$ and obtained catalysts in which the Fe^0 and Fe_2C phases that were deposited inside the support material. In another research [45] on Fe/CNF catalysts for Fischer Tropsch synthesis similar results were obtained using CNT with internal diameters up to 25 nm. As so, a plausible explanation for the location of the catalytic particles at the inner surface of the CNF could be attributed to the higher average internal diameter (up to 100 nm) of the CNF that was used in this work (Figure 2). This way, the higher inner diameter would have allowed for the penetration of the impregnation solutions through the extremities of the fibers (by capillarity, allowing for the deposition of the precursors over the CNF inner surface, resulting in the formation of Mo_2C particles that are smaller than those deposited in the outer surface.

2.3. Catalytic Activity

Table S1 (Supplementary Materials) shows the results that were obtained from the study of the effect of process conditions (time, t ; temperature, T ; pressure, P) on the guaiacol conversion and product selectivity over the synthesized catalysts, as well as of experiments with and without the CNF in order to determine the possible catalytic effects of the support material.

2.3.1. Catalyst Performance at 573 K

A set of experiments (runs 1 to 3) was undertaken at 573 K over the bare CNF support (commercial CNF pre-treated with nitric acid) and over the $\text{Mo}_2\text{C}/\text{CNF}$ catalyst for 2 h, with the purpose of gaining some insight about the reaction pathways. The results of those experiments are presented in Figure 3 (and Table S1). A longer reaction test (4 h) with the $\text{Mo}_2\text{C}/\text{CNF}$ catalyst is also included in Figure 3. The fractions of products that were identified by gas chromatography (mass balance) in those experiments were higher than 92.5%.

The conversion attained using the $\text{Mo}_2\text{C}/\text{CNF}$ catalyst was relatively low (9.7%), although corresponds to a more than 2.5-fold increase with respect to that achieved over the bare support after 2 h of reaction. The product selectivities were also significantly different in both runs. In the reaction over the bare support cresols, (*o*-cresol and *p*-cresol) were the main reaction products, followed by phenol, xylenols (2,4-dimethyl-phenol and 2,6-dimethyl-phenol), and toluene.

On the other hand, over the $\text{Mo}_2\text{C}/\text{CNF}$ the selectivity for phenol and xylenols were much higher than over the bare support, while the selectivity for cresols was much lower. In comparison with the results that were attained over the bare support, these observations seem to indicate that over the catalyst the reaction pathway favored the conversion of guaiacol into phenol and cresols, the latter being converted into xylenols by the transalkylation of methyl ($-\text{CH}_3$) groups, while disfavoring the

conversion of cresols to toluene. That is to say, the $\text{Mo}_2\text{C}/\text{CNF}$ catalyst that was used in this study was more active in disrupting aromatic ether bonds ($\text{A}-\text{O}-\text{CH}_3$) than in dehydroxylation reaction, since none of the reaction products presented methoxyl ($-\text{OCH}_3$) groups that were attached to the phenolic component. Other authors working on HDO over $\text{Co}-\text{Mo}/\text{Al}_2\text{O}_3$ catalysts at 633 K and 7 MPa [46] have previously studied the methylation and demethylation of cresols into xylenols and phenol, respectively, and concluded that these reactions comprise electrophilic substitutions involving carbonations formed from methyl groups adsorbed on acid sites over the catalyst surface. In the case of methylation, cresols adsorb on catalyst acid sites at the hydroxyl groups, while the carbocations attack the aromatic rings in the nearest accessible positions [46]. In the case of demethylation, cresols leave carbocations that are formed from the methyl groups on the catalyst surface, which can latter participate in methylation of other adsorbed molecules [46].

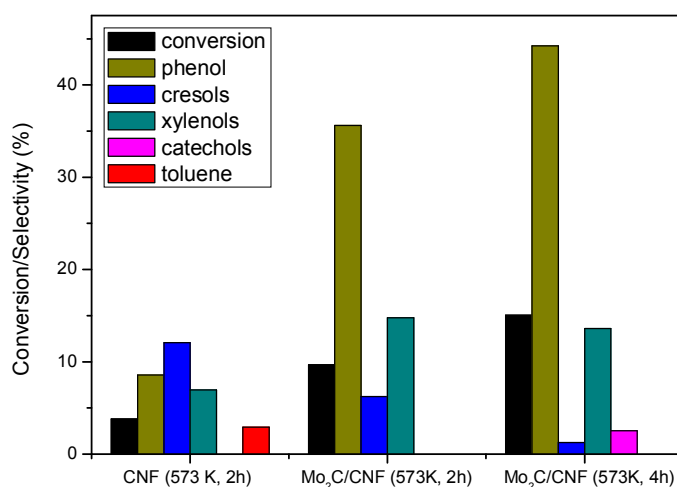


Figure 3. Conversions and product selectivities of the main reaction products during the hydrodeoxygenation of guaiacol at 573 K over the bare CNF support and the Molybdenum carbide (Mo_2C)/CNF catalysts after 2 h and 4 h of reaction.

Aiming to get a better insight on those aspects, the reaction time was prolonged up to 4 h. The results show that the higher reaction time allowed for increasing the selectivity for phenol, while the selectivity to cresols dropped abruptly. These results indicated that the increase in phenol selectivity mainly occurred by the demethylation of cresols, and was favored over its methylation into xylenols since their selectivity decreased by increasing the reaction time from 2 to 4 h (Figure 3). On the other hand, the selectivity to xylenols slightly decreased, and catechols (catechol and 3-methyl-catechol) were formed by demethylation of guaiacol, which is in agreement with the results of other authors [19] while working on similar catalysts.

The reaction pathways of the guaiacol hydrodeoxygenation over $\text{Mo}_2\text{C}/\text{CNF}$ catalyst comprise dehydration (dehydroxylation), demethylation, methylation, transalkylation, and hydrogenation steps, and have been thoroughly detailed in the literature [2,10,13,46–52]. Based on those earlier contributions, the possible reaction routes that support the experimental results at 573 K are depicted in dashed line in Figure 4.

2.3.2. Catalyst Performance at 623 K

Aiming to study the evolution of product selectivities over the $\text{Mo}_2\text{C}/\text{CNF}$ catalyst at higher guaiacol conversions, the reaction temperature was increased to 623 K. This increase in temperature was accompanied by an increase in operating pressure since the autoclave reactor was initially charged with 2 MPa of pure hydrogen (corresponding to a maximum operating pressure of 4.8 MPa).

The contribution of supports and active metals to the overall activity may be decoupled by determining the activity of the support alone, and that of the catalyst containing active metals on the

same support [53]. The results of those experiments are presented in Figure 5 (and Table S1). When the bare CNF support was used, besides phenol, cresols, and xylenols, toluene was also produced with a selectivity of 5.8%, in agreement with the results that were obtained at 573 K (run 1). The HNO₃ treated commercial CNF catalyzed the formation of toluene and catechols, since that both compounds were not detected in a blank run (Table S1). These results hinted that the CNF exerted a certain catalytic effect on the hydrodeoxygenation of guaiacol, as evidenced by the change in product selectivities, which can be related to the oxygen sites that are created by the acid treatment applied to the commercial CNF (Table 1).

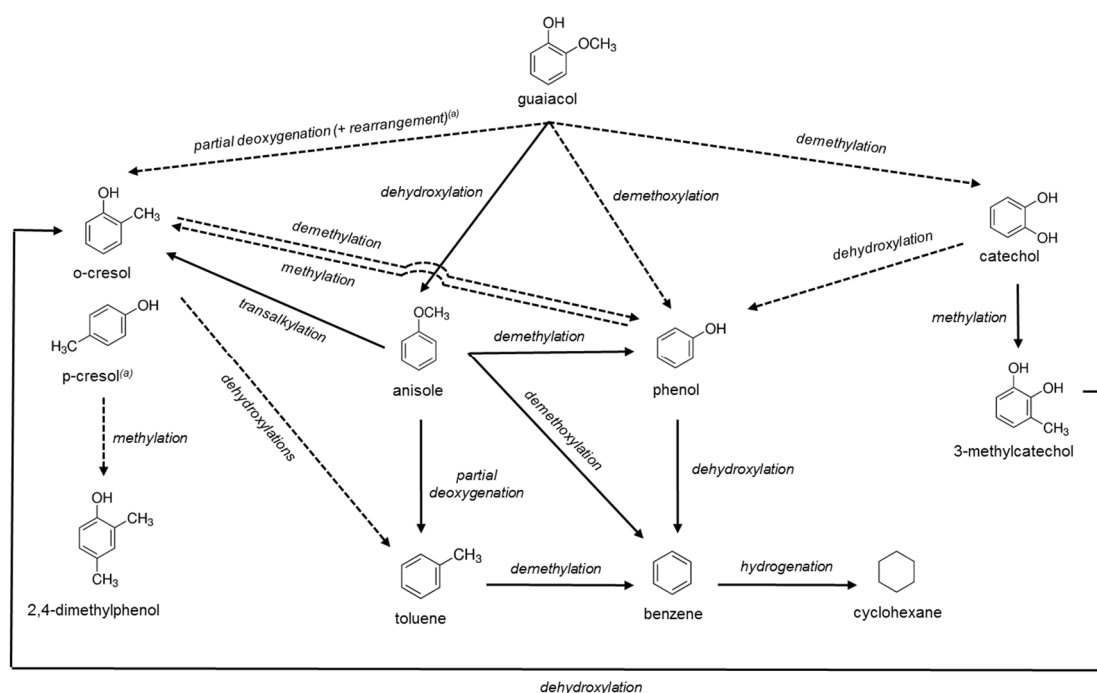


Figure 4. Scheme of the possible reaction pathways during the hydrodeoxygenation of guaiacol over the Mo₂C/CNF catalysts at 573 K (dashed lines) and at 623 K (dashed and solid lines) (adapted from [2,10,13,46–52]).

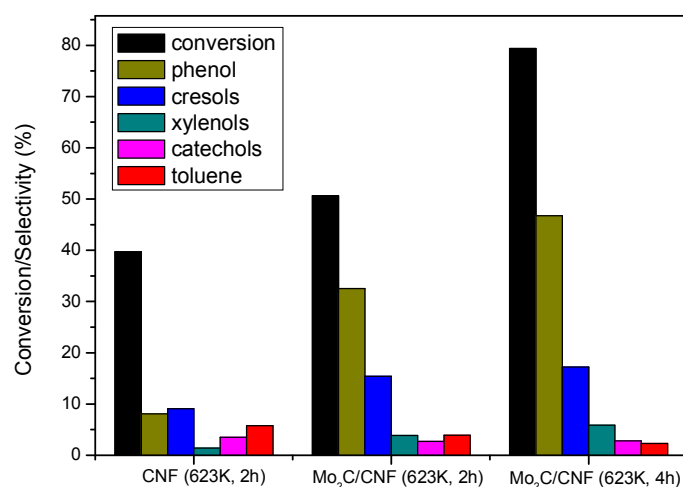


Figure 5. Conversions and product selectivities of the main reaction products during the hydrodeoxygenation of guaiacol at 623 K over the bare CNF support the Mo₂C/CNF catalyst after 2 and 4 h of reaction.

By comparing the experiments in which CNF support and the Mo₂C/CNF catalyst were used (Table 1), the conversion increased from 39.7% up to 50.6%, whereas the selectivities for phenol, cresols, and xylenols were higher. On the other hand, the selectivities for hydrocarbons and catechols in the presence of Mo₂C/CNF catalyst were lower. Moreover, anisole, which had not been detected the previous experiments (Table S1), formed by dehydroxylation of guaiacol in low quantities at 623 K [49]. No hydrogenation products were detected at 623 K, in accordance with the experiments performed under milder conditions.

Noticeably, catechols were produced at 623 K with selectivity of 2.7%, as a result of the demethylation of guaiacol, which had not been detected at 573 K. Other authors working on Mo₂C/CNF catalysts reported that the formation of phenol during HDO of guaiacol did not involve its demethylation into catechol, but instead the formation of phenol occurred by direct demethoxylation of the guaiacol [20]. However, the formation of phenol having catechol as an intermediate compound was previously reported over Mo₂C/AC catalysts [54]. Moreover, another research group [19] had previously reported that the formation of catechols in fact could occur over Mo₂C/CNF catalysts by the demethylation of guaiacol, addressing the possibility of the coexistence of the two routes above mentioned, in accordance with the results of this work. The low selectivities of catechols that were obtained in this work seem to be supported by the results of other researchers working using transition metal (Ni, Co, Fe, W, Mo) phosphides supported on silica [51] and palladium catalyst supported on zeolites [49], who stated that catechol can only be detected between HDO products when the reaction rate is low, because its conversion is almost immediate. This may explain the different reaction pathways that are reported in the literature.

On the other hand, the results that were obtained at 573 and 623 K (Figures 3 and 5) indicate that the more severe operating conditions caused a diversification of the HDO reaction pathways [52], expressed by the formation of catechol via demethylation of guaiacol as well as by the formation of anisole by its dehydroxylation. In the case of the reactions over the Mo₂C/CNF catalysts, the use of harsher operating conditions also allowed for the formation of toluene by the dehydroxylation of cresols. Alternatively, toluene may have been produced by the deoxygenation of anisole, since the last was present in the products pool with a very low selectivity (0.4%), indicating its low formation rate or its rapid conversion. Therefore, based on the literature [2,10,13,46–52], the possible reaction pathways that support the experimental results of this work are illustrated in Figure 4 (solid and dashed lines), which includes all of the compounds identified by gas chromatography (between 69.9% and 79%).

By expanding the reaction time from 2 to 4 h, the conversion increased from 50.7% to 77.4%. By far, the major products of the guaiacol HDO were phenol and cresols, as shown in Figure 5. In spite that the selectivities of all the other identified compounds have increased, the selectivity of toluene decreased and the selectivity for catechols did not change when the reaction time was increased.

Apparently, with the increase in the reaction temperature, the Mo₂C/CNF catalyst had better activity in the deoxygenation of the methoxy groups than in the removal of hydroxyl groups, while having a low hydrogenation activity. Supporting this reasoning was the fact that the selectivities for cresols and phenol were both high, while the selectivity for toluene was much higher than the summed selectivities for benzene and cyclohexane. However, it should be noted that the compounds identified by gas chromatography accounted for 79.1% and 69.9% of the HDO products in runs carried out at 2 and 4 h, respectively. This clearly indicates that a substantial part of the products pool was constituted by heavier condensation compounds that were impossible to identify by gas chromatography, in agreement with the results reported by other authors [20], being this fact more striking at largest reaction times.

For the sake of completeness, and aiming to have an estimation of the effect of pressure in the reaction with the Mo₂C/CNF catalyst, a catalytic test was performed using an initial pressure of 3.0 MPa, while the temperature was kept at 623 K and the reaction time at 2 h (Figure 6). These operating conditions caused an increase in the maximum operating pressure of 1.6 MPa, which was close to the pressure increase caused by raising the temperature from 573 K to 623 K (from 3.6 to 4.8 MPa).

The results show that the selectivities for phenol (from 32.5% to 62.6%), cresols (from 15.4% to 20.6%), and xylenols (from 3.85% to 8.60%) increased with the when the pressure was increased, while minor variations were observed on the selectivities of the other products that were identified by gas chromatography (Table S1). The results can be explained by the fact that high pressures are used in HDO to ensure adequate solubility of hydrogen in the reaction media, this way increasing its availability in the vicinity as well as on the surface of the catalyst, which in turn accelerates the reaction rates while hindering the formation of soluble higher molecular weight products than cannot be detected by GC [2]. In fact, when the pressure was increased in this work, the conversion of guaiacol increased from 50.7% to 59.1% and the identification of the compounds in the reaction pool increased from 79.1% to 88.6%, indicating that an increase in H₂ pressure inhibited the formation of heavier condensation products, in agreement with the literature [55].

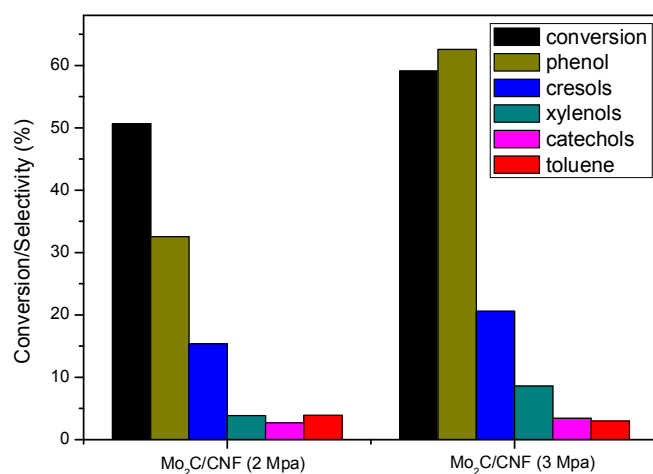


Figure 6. Conversion and product selectivities of the main reaction products during the hydrodeoxygenation of guaiacol over the Mo₂C/CNF catalyst at 623 K, 2 h reaction time and 2 and 3 Mpa H₂ pressure.

2.4. Spent Catalysts Characterization

Catalysts after HDO test were analyzed by XRD, and the diffractograms and the calculated Mo₂C crystallite size is presented in Figure 7 and Table 2, respectively.

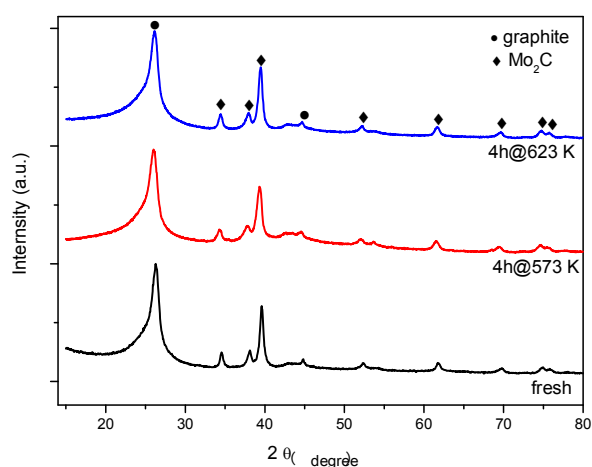


Figure 7. X-ray diffraction patterns of fresh and spent catalysts after 4 h reaction tests at 573 and 623 K.

Table 2. Mo₂C crystallite size of the fresh and spent catalysts determined by X-ray Diffraction (XRD).

Temperature (K)	Reaction Time (h)	Pressure (Mpa)	Mo ₂ C Crystallite Size (nm)
	fresh catalyst		11.2
573	2	2	9.7
573	4	2	10.2
623	2	2	7.8
623	4	2	8.6
623	2	3	7.9

No noticeable changes were observed after the catalytic tests, given that the only phases that were detected were Mo₂C, and no MoO_x were observed. Besides this, Mo₂C crystallite size presented slightly lower values than in the fresh catalysts, more accentuated at higher temperature, which evidenced that no sintering takes place during the reaction.

3. Materials and Methods

3.1. Chemicals

Commercial CNF (PR-24 XT-PS, Pyrograf[®], Cedarville, OH, USA) were used as catalyst support material, while ammonium heptamolybdate hexahydrate (Sigma Aldrich[®], St. Louis, MO, USA), was used as metal precursors. Guaiacol (>99%, Sigma Aldrich[®]) was used as model compound of fast pyrolysis bio-oil, and decane (>99%, Sigma Aldrich[®]) was used as reaction solvent. Pure nitrogen (99%, Air Liquid, Paris, France) was used for purging the reactor and pure hydrogen (99%, Air Liquid) was used as reactant. Ethanol (>99.8%, Sigma Aldrich[®]) was used as solvent for rinsing the catalyst after its separation from the reaction products and nitric acid (>90%, Sigma Aldrich[®]) was used in CNF pretreatment.

3.2. Catalyst Preparation and Characterization

The as received commercial nanofibers (CNF) were functionalized, aiming to create oxygen groups and facilitating the metal dispersion on the CNF surface, as detailed in previous works [27,28]. Succinctly, the CNF were treated for 2 h in diluted boiling nitric acid (HNO₃) using the following proportions: 2 g CNF/50 mL HNO₃/150 mL distilled water. The so treated nanofibers were separated by vacuum filtration from the diluted acid using a cellulose filter (0.2 μm porosity and 8 cm diameter, Whatman[®], Maidstone, UK), rinsed with distilled water until the filtrate has reached pH = 7, and oven dried for 12 h.

The catalyst was prepared by incipient wetness impregnation, followed by carbothermal reduction. The dried CNF were impregnated with ammonium heptamolybdate hexahydrate (Sigma Aldrich[®]) in one step, and then oven dried for 12 h, followed by carburization in flowing hydrogen (100 mL/min) using a heating rate of 10 K/min up to 1023 K, maintained for two additional hours at this set point temperature. Then, the catalyst was cooled down to room temperature under pure nitrogen flow and passivated in 1% O₂ in N₂ (Air Liquid) for 2 h.

Phase composition and structure of supports and fresh catalyst were determined by X-ray Diffraction (XRD), in a D8 Advance Series 2 diffractometer (Bruker, Billerica, MA, USA) equipped with a Ni-filtered Cu Kα radiation and a secondary graphite monochromator, using a θ–2θ configuration. Bulk morphology was studied by Transmission Electron Microscopy (TEM) using a Jeol 2011 microscope (JEOL, Tokyo, Japan) with a LaB₆ gun operating at 200 KV, and coupled to Energy-Dispersive X-ray Spectroscopy (EDX). Crystallite size was determined by XRD and TEM. The textural properties were measured by N₂ adsorption at 77 K in a Micromeritics Tristar apparatus (Micromeritics Instrument Corp., Norcross, GA, USA). Specific surface area and pore volume were calculated by applying the BET method to the N₂ adsorption isotherm and the pore size distribution was calculated by the BJH method based on the desorption branch of the isotherm. Temperature

Programmed Desorption (TPD) was performed to evaluate the CO and CO₂ eluted from pretreated (CNF) in an AutoChem II 2920 apparatus (Micromeritics Instrument Corp., Norcross, GA, USA) under constant Argon flow (50 mL/min) using a heating rate of 10 K/min up to 1273 K. The eluted gas was analyzed by mass spectroscopy. The total amount of CO and CO₂ released was calculated by integrating the area under the concentration versus volume curve. Oxygen content was determined from the amount of CO and CO₂ released.

3.3. Catalytic Testing and Product Characterization

The effects of operating conditions (temperature and pressure) and reaction time (2, 4 and 6 h) on the conversion of guaiacol and products selectivity were studied.

The catalytic tests were performed in a 100 mL high pressure batch reactor (Parker Autoclave Engineers, Erie, PA, USA). Prior each run, the autoclave reactor was loaded with 1.2 mL (3 wt %) of guaiacol in 40 mL of decane (97 wt %), and 0.2 g of catalyst. The reactor was purged at an ambient temperature first with pure nitrogen, and then with pure hydrogen. Afterwards, the reactor was loaded with 2 MPa of hydrogen (or 3 MPa in run 9), and heated to the reaction temperature while stirring at 300 rpm (in order to minimize reaction during heating). Once the reaction temperature has been achieved, the stirring was increased to 1000 rpm and the reaction time counting was initiated. The reaction was stopped by decreasing the stirring to 300 rpm and cooling the reactor with compressed air until ambient temperature has been achieved. Blank experiments both with and without CNF were performed in order to distinguish eventual catalytic effect of the bare CNF support from the effect of reaction temperature on conversion of guaiacol and selectivity to HDO products.

Conversion of guaiacol (X) and product selectivity (S) were calculated using Equations (1) and (2) as follows.

$$X(\%) = \frac{C_i - C_f}{C_i} \times 100 \quad (1)$$

$$S(\%) = \frac{C_{pi}}{C_i - C_f} \times 100 \quad (2)$$

where C_i is the initial concentration guaiacol (mmol/mL), C_f is the final concentration of guaiacol in the reaction products (mmol/mL), and C_{pi} is the concentration of product i (mmol/mL). The operating conditions used during the HDO experiments with the three synthesized catalysts are presented in Table S1.

After each experiment, the catalyst was separated by gravity filtration from the reaction products using a cellulose filter (0.2 μ m porosity and 4 cm diameter, Whatman[®]). The so recovered catalyst was then rinsed with 50 mL pure ethanol, and the obtained filtrate was chemically analyzed aiming the detection of intermediate reaction compounds. The characterization of reaction products was performed by GC-FID (Perkin Elmer[®], Waltham, MA, USA) and GC-MS (Perkin Elmer[®]). For that, aliquots of the catalyst free liquid were collected using a syringe assembled with a filter (Whatman[®]) and injected directly in the chromatographic analyzers.

4. Conclusions

A Mo₂C catalyst supported on commercial CNF was tested in the HDO of guaiacol, the major reaction products were cresol and phenol, followed by xylenols and toluene. The increase in the reaction temperature up to 623 K use of more severe operating conditions in the HDO of guaiacol caused a diversification in the reaction pathways, and consequently, in the selectivity to products, allowing for demethoxylation reactions being almost absent at 573 K.

The etching of carbonaceous materials involving molybdenum is reported in the present work for the first time, and is possibly related with the formation of molybdenum carbides by carburization of in hydrogen atmosphere.

The formation of catechols was observed over all of the catalysts that were prepared for this work, indicating that the formation of phenol may occur by the demethylation of guaiacol, followed by dehydroxylation of catechol, together with other reaction pathways, including direct guaiacol demethoxylation and demethylation of cresols.

The increase in the HDO of guaiacol caused an increase in conversion as well as in the reaction products identifiable by GC-MS, while reducing coking.

Supplementary Materials: The following are available online at <http://www.mdpi.com/2073-4344/8/4/127/s1>, Table S1: Operating conditions, conversions and product selectivities during the hydrodeoxygenation of guaiacol over the Mo₂C/CNF catalyst.

Acknowledgments: This work was funded by FEDER and the Spanish Economy and Competitiveness Ministry (MINECO) (ENE2014-52189-C02-01-R and ENE2017-83854-R). Elba Ochoa thanks for the award of her PhD under the frame of this project. J.L.P. thanks MINECO for his Ramon y Cajal research contract (RYC-2013-12494). Rui Moreira is extremely grateful to ICB-CSIC for partially financing living costs during his short term mission. The authors are also grateful to the PhD Student Esther Frecha for helping in the GC-FID analysis, and to Daniel Torres for helping in the interpretation of results.

Author Contributions: R.M. prepared the catalysts, performed the catalytic tests and analyzed the data, with the help of E.O. and J.L.P., E.O. carried out the characterization of the reaction products by GC and GC/MS. R.M. and J.L.P. wrote the manuscript. J.L.P. and I.S. provided the means needed for the realization of this work. A.P. participated as assessor and contributed to the discussion of the results. All authors read and approved the manuscript.

Conflicts of Interest: The authors declare no conflict of interest. The founding sponsors had no role in the design of the study; in the collection, analyses, or interpretation of data; in the writing of the manuscript, and in the decision to publish the results.

References

1. Lu, Q.; Li, W.-Z.; Zhu, X.-F. Overview of fuel properties of biomass fast pyrolysis. *Energy Convers. Manag.* **2009**, *50*, 1376–1383. [[CrossRef](#)]
2. Mortensen, P.; Grunwaldt, J.; Jensen, P.; Knudsen, K.; Jensen, A. A review of catalytic upgrading of bio-oil to engine fuels. *Appl. Catal. A Gen.* **2011**, *407*, 1–19. [[CrossRef](#)]
3. Butler, E.; Devlin, G.; Meier, D.; McDonnell, K. A review of recent laboratory research and commercial developments in fast pyrolysis and upgrading. *Renew. Sustain. Energy Rev.* **2011**, *15*, 4171–4186. [[CrossRef](#)]
4. He, V.; Wang, X. Hydrodeoxygenation of model compounds and catalytic systems for pyrolysis bio-oils upgrading. *Catal. Sustain. Energy* **2013**, *1*, 28–52. [[CrossRef](#)]
5. Venderbosch, R.; Ardiyanti, A.; Wildschut, J.; Oasmaa, A.; Heeres, H. Stabilization of biomass-derived pyrolysis oils. *J. Chem. Technol. Biotechnol.* **2010**, *85*, 674–686. [[CrossRef](#)]
6. Choi, J.; Bugli, G.; Djéga-Mariadassou, G. Influence of the Degree of Carburization on the Density of Sites and Hydrogenating Activity of Molybdenum Carbides. *J. Catal.* **2000**, *193*, 238–247. [[CrossRef](#)]
7. Nguyen, T.; Lee, T.; Safinski, T.; Adesina, A. Structural evolution of alumina supported Mo–W carbide nanoparticles synthesized by precipitation from homogeneous solution. *Mater. Res. Bull.* **2005**, *40*, 149–157. [[CrossRef](#)]
8. Furimsky, E. Metal carbides and nitrides as potential catalysts for hydroprocessing. *Appl. Catal. A Gen.* **2003**, *40*, 1–28. [[CrossRef](#)]
9. Boullosa-Eirasa, S.; Lødeng, R.; Bergem, H.; Stöcker, M.; Hannevold, L.; Blekkan, E. Catalytic hydrodeoxygenation (HDO) of phenol over supported molybdenum carbide, nitride, phosphide and oxide catalysts. *Catal. Today* **2014**, *223*, 44–53. [[CrossRef](#)]
10. Furimsky, E. Catalytic hydrodeoxygenation. *Appl. Catal. A Gen.* **2000**, *199*, 147–190. [[CrossRef](#)]
11. Politi, R.; Vines, F.; Rodriguez, J.; Illas, F. Atomic and electronic structure of molybdenum carbide phases: Bulk and low Miller-index surfaces. *Phys. Chem. Chem. Phys.* **2013**, *15*, 12617–12625. [[CrossRef](#)] [[PubMed](#)]
12. Posada-Pérez, S.; Viñesa, F.; Valero, R.; Rodriguez, J.; Illas, F. Adsorption and dissociation of molecular hydrogen on orthorhombic β -Mo₂C and cubic δ -MoC (001) surfaces. *Surf. Sci.* **2017**, *656*, 24–32. [[CrossRef](#)]
13. Dongil, A.; Ghampson, I.; García, R.; Fierro, J.; Escalona, N. Hydrodeoxygenation of guaiacol over Ni/carbon catalysts: Effect of the support and Ni loading. *RSC Adv.* **2016**, *6*, 2611–2623. [[CrossRef](#)]

14. Serp, F.; Corrias, M.; Kalck, P. Carbon nanotubes and nanofibers in catalysis. *Appl. Catal. A Gen.* **2003**, *253*, 337–358. [[CrossRef](#)]
15. Vieira, R. Carbon Nanofibers as Macro-Structured Catalytic Support. In *Nanofibers*; InTech: Rijeka, Croatia, 2010; pp. 1–12.
16. Jong, K.; Gues, J. Carbon nanofibers: Catalytic synthesis and applications. *Catal. Rev. Sci. Eng.* **2000**, *42*, 481–510. [[CrossRef](#)]
17. Park, C.; Anderson, P.; Chambers, A.; Tan, C.; Hidalgo, R.; Rodriguez, N. Further Studies of the Interaction of Hydrogen with Graphite Nanofibers. *J. Phys. Chem. B* **1999**, *103*, 10572–10581. [[CrossRef](#)]
18. Rodriguez-Reinoso, F. The role of carbon materials in heterogeneous catalysis. *Carbon* **1998**, *36*, 159–175. [[CrossRef](#)]
19. Santillan-Jimenez, E.; Perdu, M.; Pace, R.; Morgan, T.; Crocker, M. Activated Carbon, Carbon Nanofiber and Carbon Nanotube Supported Molybdenum Carbide Catalysts for the Hydrodeoxygenation of Guaiacol. *Catalysts* **2015**, *5*, 424–441. [[CrossRef](#)]
20. Jongerius, A.; Gosselink, R.; Dijkstra, J.; Bitter, J.; Bruijninx, P.; Weckhuysen, B. Carbon Nanofiber Supported Transition-Metal Carbide Catalysts for the Hydrodeoxygenation of Guaiacol. *ChemCatChem* **2013**, *5*, 2964–2972. [[CrossRef](#)]
21. Mordenti, D.; Brodzki, D.; Djéga-Mariadassou, G. New Synthesis of Mo₂C 14 nm in Average Size Supported on a High Specific Surface Area Carbon Material. *J. Solid State Chem.* **1998**, *141*, 114–120. [[CrossRef](#)]
22. Chaudhury, S.; Mukerjee, S.; Vaidya, V.; Venugopal, V. Kinetics and mechanism of carbothermic reduction of MoO₃ to Mo₂C. *J. Alloys Compd.* **1997**, *261*, 105–113. [[CrossRef](#)]
23. Deutsch, K.; Shanks, B. Hydrodeoxygenation of lignin model compounds over a copper chromite catalyst. *Appl. Catal. A Gen.* **2012**, *447*, 144–150. [[CrossRef](#)]
24. Zhou, J.; Sui, Z.; Zhua, J.; Li, P.; Chen, D.; Dai, Y.; Yuan, W. Characterization of surface oxygen complexes on carbon nanofibers by TPD, XPS and FT-IR. *Carbon* **2007**, *45*, 785–796. [[CrossRef](#)]
25. Zhuang, Q.; Kyotani, T.; Tomita, A. DRIFT and TK/TPD Analyses of Surface Oxygen Complexes Formed during Carbon Gasification. *Energy Fuels* **1994**, *8*, 714–718. [[CrossRef](#)]
26. Boehm, H. Surface oxides on carbon and their analysis: A critical assessment. *Carbon* **2002**, *40*, 145–149. [[CrossRef](#)]
27. Pinilla, J.; Purón, H.; Torres, D.; Llobet, S.; Moliner, R.; Suelves, I.; Millana, M. Carbon nanofibres coated with Ni decorated MoS₂ nanosheets as catalyst for vacuum residue hydroprocessing. *Appl. Catal. B Environ.* **2014**, *148–149*, 357–365. [[CrossRef](#)]
28. Pinilla, J.; Purón, H.; Torres, D.; Suelves, I.; Millana, M. Ni-MoS₂ supported on carbon nanofibers as hydrogenation catalysts: Effect of support functionalization. *Carbon* **2015**, *81*, 574–586. [[CrossRef](#)]
29. Guil-López, R.; Nieto, E.; Botas, J.; Fierro, J. On the genesis of molybdenum carbide phases during reduction-carburization reactions. *J. Solid State Chem.* **2012**, *190*, 285–295. [[CrossRef](#)]
30. Reddy, K.; Rao, T.; Revathi, J.; Joardar, J. Structural stability of α/β -Mo₂C during thermochemical processing. *J. Alloys Compd.* **2010**, *494*, 386–391. [[CrossRef](#)]
31. Dubois, J.; Epicier, T.; Esnouf, C.; Fantozzi, G. Neutron powder diffraction studies of transition metal hemicarbides M₂C_{1-x}—I. Motivation for a study on W₂C and Mo₂C and experimental background for in situ investigation at elevated temperature. *Acta Metal.* **1998**, *36*, 1891–1901. [[CrossRef](#)]
32. Dubois, J.; Epicier, T.; Esnouf, C.; Fantozzi, G. Neutron powder diffraction studies of transition metal hemicarbides M₂C_{1-x}—II. In situ high temperature study on W₂C_{1-x} and Mo₂C_{1-x}. *Acta Metal.* **1998**, *36*, 1903–1921.
33. Araujo, C.; Souza, C.; Maia, L.; Souto, M.; Barbosa, C. On the synthesis of molybdenum carbide with cobalt addition via gas-solid reactions in a CH₄/H₂ atmosphere. *Braz. J. Chem. Eng.* **2016**, *3*, 577–588. [[CrossRef](#)]
34. Stellwagen, D.; Bitter, J. Structure–performance relations of molybdenum and tungsten carbide catalysts for deoxygenation. *Green Chem.* **2015**, *17*, 582–593. [[CrossRef](#)]
35. Baaziz, W.; Melinte, G.; Ersen, O.; Pham-Huu, C.; Janowska, I. Effect of nitriding/nanostructuring of few layer graphene supported iron-based particles; catalyst in graphene etching and carbon nanofilament growth. *Phys. Chem. Chem. Phys.* **2014**, *16*, 15988–15993. [[CrossRef](#)] [[PubMed](#)]
36. Papaefthimiou, V.; Florea, I.; Baaziz, W.; Janowska, I.; Doh, W.; Begin, D.; Blume, R.; Knop-Gericke, A.; Ersen, O.; Pham-Huu, C.; et al. Effect of the Specific Surface Sites on the Reducibility of α -Fe₂O₃/Graphene Composites by Hydrogen. *J. Phys. Chem. Chem. Phys.* **2013**, *117*, 20313–20319. [[CrossRef](#)]

37. Datta, S.; Strachan, D.; Khamis, S.; Johnson, A. Crystallographic Etching of Few-Layer Graphene. *Nano Lett.* **2008**, *7*, 1912–1915. [[CrossRef](#)] [[PubMed](#)]
38. Ramasse, Q.; Zan, R.; Ursel Bangert, U.; Boukhalov, D.; Son, Y.; Novoselov, K. Direct Experimental Evidence of Metal-Mediated Etching of Suspended Graphene. *ACS Nano* **2012**, *6*, 4063–4071. [[CrossRef](#)] [[PubMed](#)]
39. Schäffel, F.; Warner, J.; Bachmatiuk, A.; Rellinghaus, B.; Büchner, B.; Schultz, L.; Rummeli, M. Shedding Light on the Crystallographic Etching of Multi-Layer Graphene at the Atomic Scale. *Nano Res.* **2009**, *2*, 695–705. [[CrossRef](#)]
40. Schäffel, F.; Warner, J.; Bachmatiuk, A.; Rellinghaus, B.; Büchner, B.; Schultz, L.; Rummeli, M. On the catalytic hydrogenation of graphite for graphene nanoribbon fabrication. *Phys. Status Solidi B* **2009**, *246*, 2540–2544. [[CrossRef](#)]
41. Wang, R.; Wang, J.; Gong, H.; Luo, Z.; Zhan, D.; Shen, Z.; Thong, J. Cobalt-Mediated Crystallographic Etching of Graphite from Defects. *Small* **2012**, *8*, 2515–2523. [[CrossRef](#)] [[PubMed](#)]
42. Campos, J.; Manfrinato, V.; Sanchez-Yamagishi, J.; Kong, J.; Jarillo-Herrero, P. Anisotropic Etching and Nanoribbon Formation in Single-Layer Graphene. *Nano Lett.* **2009**, *9*, 2600–2604. [[CrossRef](#)] [[PubMed](#)]
43. Xiong, H.; Motchelaho, M.; Moyo, M.; Jewell, L.; Coville, N. Cobalt catalysts supported on a micro-coil carbon in Fischer–Tropsch synthesis: A comparison with CNTs and CNFs. *Catal. Today* **2013**, *214*, 50–60. [[CrossRef](#)]
44. Chen, W.; Fan, Z.; Pan, X.; Bao, X. Effect of Confinement in Carbon Nanotubes on the Activity of Fischer–Tropsch Iron Catalyst. *J. Am. Chem. Soc.* **2008**, *130*, 9414–9419. [[CrossRef](#)] [[PubMed](#)]
45. Abbaslou, R.; Tavassoli, A.; Soltan, J.; Dalai, A. Iron catalysts supported on carbon nanotubes for Fischer–Tropsch synthesis: Effect of catalytic site position. *Appl. Catal. A Gen.* **2009**, *367*, 47–52. [[CrossRef](#)]
46. Wandas, R.; Surygata, J.; Sliwka, E. Conversion of cresols and naphthalene in the hydroprocessing of three-component model mixtures simulating fast pyrolysis tars. *Fuel* **1996**, *75*, 687–694. [[CrossRef](#)]
47. Saidi, M.; Samimi, F.; Karimipourfard, D.; Nimmanwudipong, T.; Gates, B.; Rahimpour, M. Upgrading of lignin-derived bio-oils by catalytic hydrodeoxygenation. *Energy Environ. Science* **2014**, *7*, 103–129.
48. Nimmanwudipong, T.; Aydin, C.; Lu, J.; Ron, C.; Runnebaum, R.; Brodwater, K.; Browning, N.; Block, D.; Gates, B. Selective Hydrodeoxygenation of Guaiacol Catalyzed by Platinum Supported on Magnesium Oxide. *Catal. Lett.* **2012**, *142*, 1190–1196. [[CrossRef](#)]
49. Lee, H.; Kim, H.; Yu, M.; Ko, C.; Jeon, J.; Jae, J.; Park, S.; Jung, S.; Park, Y. Catalytic Hydrodeoxygenation of Bio-oil Model Compounds over Pt/HY Catalyst. *Nat. Sci. Rep.* **2016**, *6*, 1–8. [[CrossRef](#)] [[PubMed](#)]
50. Zhao, C.; He, J.; Lemonidou, A.; Li, X.; Lercher, J. Aqueous-phase hydrodeoxygenation of bio-derived phenols to cycloalkanes. *J. Catal.* **2011**, *280*, 8–16. [[CrossRef](#)]
51. Zhao, H.; Li, D.; Bui, P.; Oyama, S. Hydrodeoxygenation of guaiacol as model compound for pyrolysis oil on transition metal phosphide hydroprocessing catalysts. *Appl. Catal. A Gen.* **2011**, *391*, 305–310. [[CrossRef](#)]
52. Zhao, C.; Camaioni, D.; Lercher, J. Selective catalytic hydroalkylation and deoxygenation of substituted phenols to bicycloalkanes. *J. Catal.* **2012**, *288*, 92–103. [[CrossRef](#)]
53. Furimsky, E. *Carbons and Carbon-Supported Catalysts in Hydroprocessing*; The Royal Society of Chemistry, IMAF Group: Ottawa, ON, Canada, 2008; pp. 12–126.
54. Ma, R.; Cui, K.; Yang, L.; Ma, X.; Li, Y. Selective catalytic conversion of guaiacol to phenols over a molybdenum carbide catalyst. *Chem. Commun.* **2015**, *51*, 10299–10301. [[CrossRef](#)] [[PubMed](#)]
55. Kwon, K.; Mayfield, H.; Marolla, T.; Nichols, B.; Mashburn, M. Catalytic Deoxygenation of Liquid Biomass for Hydrocarbon Fuels. *Renew. Energy* **2011**, *36*, 907–1015. [[CrossRef](#)]

